Design and Characterization of E-Field Probes for Lossy Media

Katja Poković, Thomas Schmid, Andreas Christ and Niels Kuster

Abstract—Since ensuring compliance with safety limits has lately become a product liability issue, another quality of requirements is placed on instrumentation and procedures for experimental dosimetry with respect to reliability and overall precision, as compared to similar tests (e.g., EMC, etc.). The highly nonhomogeneous field distributions encountered in lossy biological tissue pose great demands on the small isotropic E-field probes commonly used for local dosimetry. Field disturbance, spherical isotropy and spatial resolution are crucial parameters for assessing the probe performance/uncertainty in a specific application. While many papers describe the characteristics of the sensors and the lines in small E-field probes, little literature is available on the various field distortions occurring between the incident field and the fields measured by the probe sensors. Data on commercially available probes are generally scarce and the probes are often used in an inappropriate manner, resulting in large measurement uncertainties. The paper shows the influences of the mechanical construction materials, signal detection and readout on the probe characteristics with an emphasis on the field effects and coupling of probes used in lossy media such as: field distortion by the probe (e.g.,boundary effects); field deflection inside the probe (e.g., eddy current effects, spatial resolution); field detection and readout. In addition, design criteria for minimizing the probe errors are discussed.

I. INTRODUCTION

The unit of interest in RF and microwave dosimetry is the specific absorption rate (SAR) defined as the absorbed power per tissue mass:

$$SAR = \frac{dP}{dm} = \frac{\sigma}{\rho}E^2 = c\frac{dT}{dt} \qquad (1)$$

where σ is the conductivity, ρ the density and c the specific heat of the tissue at the site of measurement, E is the Hermitian magnitude of the local electric field vector and dT/dt the time derivative of the temperature. Both temperature rise and induced E-field measurements can be used to assess the SAR inside the exposed tissue. While temperature measurements are scalar measurements with probes that can be easily calibrated, E-field measurements have a much higher sensitivity, are undisturbed by heat exchange processes in the tissue and are therefore more favorable for dosimetric evaluations of various RF transmitters.

The high losses in biological tissue, the tissue dimensions in the range of the wavelengths and the common exposure in the near-field of radiators produce E-fields which are highly anisotropic and unpredictable. This poses high requirements for field probes with respect to isotropy, field disturbance and spatial resolution. The ideal probe would consist of three orthogonal Hertzian dipole sensors directly

The authors are with the Swiss Federal Institute of Technology, 8092 Zürich, Switzerland

implanted at the same location in the tissue. However, classical E-field probes consist of dipole sensors of finite length which are mounted on substrates, displaced from the probe's center and encapsulated by dielectric materials. Detector diodes at the dipole gap rectify the RF signal, and resistive lines connect the sensors to the data acquisition system. Due to these construction requirements, the output of an actual probe is not only proportional to the field strength (or the square of the field strength) but also depends on other parameters of the field or the measurement setup such as:

- frequency, modulation and field strength
- field polarization and direction
- field gradient
- media boundaries in the probe vicinity
- other field sources (noise, static fields, ELF fields, etc.)
- other physical influences (temperature, etc.)

During calibration, the probe output is assessed in one or several specific situations, where all influencing parameters are well controlled and specified within the calibration uncertainty. Since conditions during measurements might be significantly different than those of the calibration setup, the relative probe deviations and uncertainties with respect to all influencing parameters must be specified in order to calculate the total probe uncertainty for a specific measurement task.
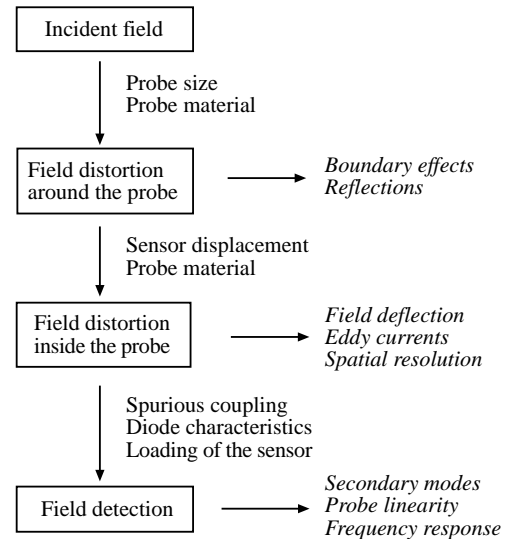

Fig. 1. An overview of which construction details affect which part of the probe performance.

Because no probe can cover all possible situations, the parameter limitations (e.g., frequency range, maximum field strength) for the specified uncertainties must be

known. If a parameter can be reconstructed from the probe output (e.g., the RF voltage at the diode), the corresponding probe specification can be used to compensate the probe deviation in the evaluation system (e.g., linearization of the diode compression).

The purpose of this paper is to analyze how dosimetric probes immersed in lossy media affect the field measurement and to derive design criteria and evaluation procedures to minimize the uncertainty of the SAR assessment. In Fig.1 an overview of the significant probe construction details and their effect on probe performance is given.

The three dosimetric probes used in the investigation are shown in Fig.2. All probes are optimized for dosimetry in solutions with high permittivity and use a triangular sensor configuration.
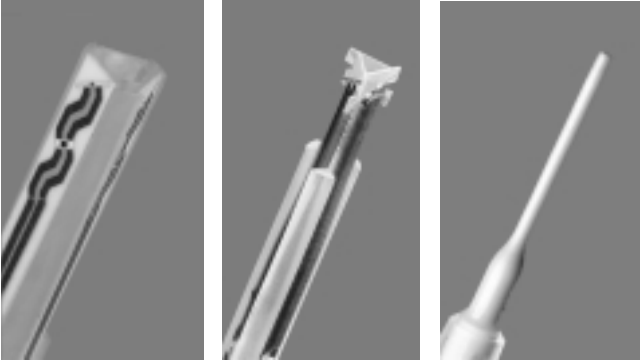

Fig. 2. Different designs of E-field probes used for dosimetric measurements: probe A (left), probe B (middle), probe C (right). Probes A and B are shown without the encapsulation. See Table I for dimensions.

A review of the different sensor configurations is given in [1]. The geometrical specifications of the probes are summarized in Table I. Probes A (ET3D) and B (ES3D) are used for general dosimetry and compliance testing of MTE. Probe A has already been presented in [2]. Probe C (ET1D) has only one angled sensor and is mainly used for dosimetry in cell dishes and small animals. The three field components are measured sequentially by rotating the probe around its axis. A high precision 6-axes robot positioner is used for the measurements, allowing probe rotations in multiple axes with a positioning uncertainty below 0.1 mm at the probe tip.

TABLE I
GEOMETRICAL SPECIFICATIONS OF DOSIMETRIC E-FIELD PROBES.

Probe	Tip diameter [mm]	Sensor offset from tip [mm]	Sensor displacement from center [mm]	Sensor length [mm]
A	6.8	2.7	1.6	3
B	3.9	2.7	0.6	3
C	1.0	0.5	0.0	0.8

Numerical simulations using Finite Difference Time Domain (FDTD) and Multiple Multipole (MMP) codes were additionally used to analyze probe performance. In Fig.3

the numerical model of probe A is shown. The probe was simulated using a graded mesh with the smallest grid spacing of 0.125 mm at the probe tip. The probe response was assessed by calculating the gap voltage over the modeled dipoles. A simple homogeneous probe model with 0.5 mm grid spacing was used to visualize the field effects qualitatively.
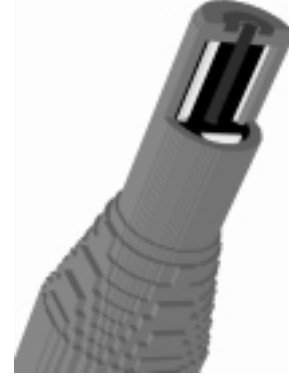

Fig. 3. Numerical model (FDTD) of probe A.

II. FIELD DISTORTION AROUND THE PROBE

The difference in the dielectric parameters between the probe materials and the surrounding media produces a disturbance of the field in the immediate vicinity of the probe. In Fig.4 the scattered field caused by probe A in brain tissue simulating liquid at 900 MHz (ε=42.5, σ=0.85) is shown as a percentage of the incident field at the probe tip. It can be seen that the disturbance is small for the frontal plane wave incidence (Fig.4 left) and largest for the lateral incidence with the incident E-field parallel to the probe axis (Fig.4 right). During probe calibration in lossy media the field disturbance is accounted for. However, any additional disturbance of the scattered field can strongly affect the probe performance (e.g., multiple reflections between the probe and nearby objects).
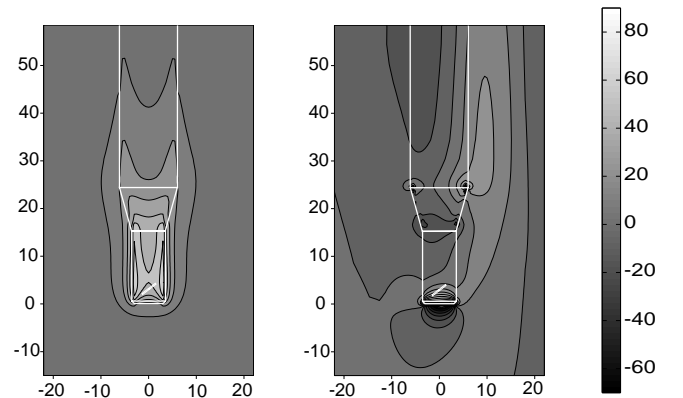

Fig. 4. Field disturbance as a percentage of the incident field of the around the probe A (left: frontal incidence with E-field normal to the probe axis; right: lateral incidence with E-field parallel to the probe axis). Dimensions are in mm.

A. Boundary Effects

If a material boundary passes through the area of the field disturbance around the probe, the field inside the probe will interact with the field at the boundary (multiple reflections) and the probe sensitivity can change dramatically. These effects depend not only on the initial field and the probe, but also on the properties of the boundary (orientation, curvature, distance to the probe, permittivities on both sides of the boundary, etc). The number of parameters make a general compensation of the boundary effects impossible, thus seriously impairing the use of E-field probes near boundaries in multilayered anatomical phantoms.

The boundary effects of the three probes were investigated for the common case of measurement near the bottom of liquid-filled shell phantoms (used for compliance testing of mobile phones) where the fields at the surface are of main concern. The SAR values at the surface cannot be measured directly and must be extrapolated from measurments at various distances. Often highly unisotropic fields near the shell surface would introduce large uncertainties if the field at the surface is extrapolated from measurements far above the surface (see Fig.7). On the other hand, measurements near the surface suffer from the boundary effects. Fig.5 shows the measured SAR near the boundary in the analytical setup used for probe calibrations [3]. The z-axis indicates the distance of the sensor centers from the liquid boundary; at the lowest measured point the probe is touching the boundary.
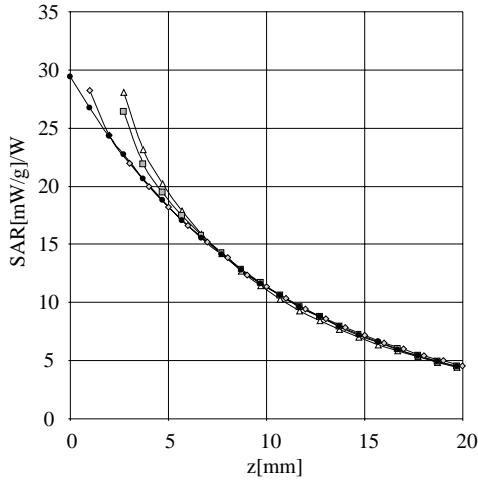

Fig. 5. SAR distribution near the boundary assessed with an analytical solution (●), measured with probe A (△), probe B (□) and probe C (◇).

An FDTD simulation of the boundary effect for probe A is given in Fig.6 for the distances of 3 mm (z = 5.7 mm) and 1 mm (z = 3.7 mm) between probe tip and boundary. Displayed is the additional field disturbance due to the boundary as a percentage of the incident field at the probe tip.

Both measurements and simulation show an enhanced sensitivity in the immediate vicinity of the boundary. The
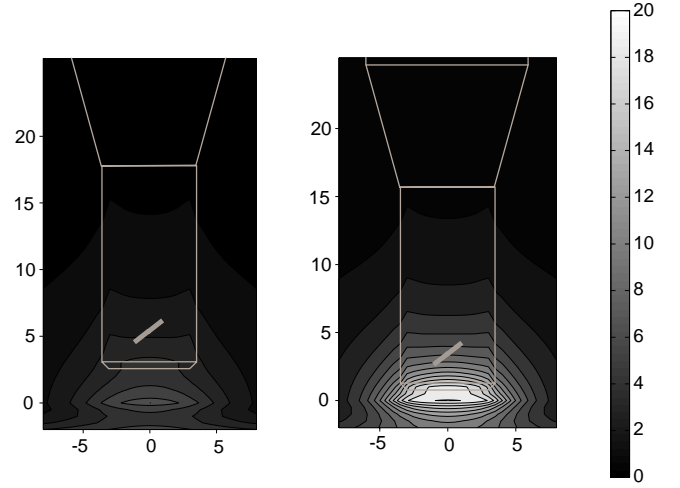

Fig. 6. Field distortion as a percentage of the incident field due to the boundary at 3 mm (left) and 1 mm (right) distance for a frontal incident plane wave at 900 MHz. Dimensions are in mm.

effect strongly depends on the probe dimensions and disappears with increasing distance from the boundary. The sensitivity can be approximately given as:

$$S \approx S_o + S_b exp(-\frac{z}{a})cos(\pi\frac{z}{\lambda}) \qquad (2)$$

Since the decay of the boundary effect dominates for small probes (a $<<\lambda$), the cos-term can be omitted. Factors S_b and a can be assessed during the probe calibration and used for numerical compensation of the boundary effect. Several simulations and measurements confirmed that the compensation is valid for different field and boundary configurations. As a reference for the undisturbed field, analytical solutions, numerical simulations or measurements with probe C were used. In Fig.7 the measured boundary effect for an extreme field situation is shown. For probe A the boundary effect was compensated using the factors assessed during the calibration. The values were then extrapolated to the surface using a standard 4th order polynomial extrapolation and show good agreement with the values measured with probe C.
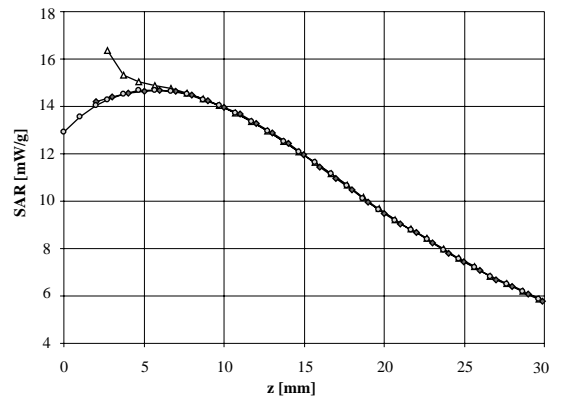

Fig. 7. Example of an extreme field situation near the phantom boundary. SAR measured with probe A (△) and probe C (◇), as well as using advanced evaluation of the data measured with probe A (○).

The simple compensation procedure can largely reduce the probe uncertainty near boundaries. It works well as long as:

- the boundary curvature is small
- the probe axis is angled less than 30° to the boundary normal
- the distance between probe and boundary is larger than 25% of the probe diameter
- the probe is symmetric (all sensors have the same offset from the probe tip)

These conditions can be easily fulfilled using an automatic field scanning system and simple shell phantoms [2].

III. Field Distortion inside the Probe

The sensors in E-field probes actually measure the local E-field inside the probe. Since the probe materials generally have other dielectric properties than the surrounding material, the internal fields differ in magnitude and direction from the external fields. These deviations strongly depend not only on the dielectric properties of both the surrounding media and the probe materials, but also on the probe construction and the sensor location in the probe.

A. Field deflection

Due to the symmetrical configuration of probes with respect to the probe axis, the isotropy for frontal incident plane waves (with the E-field always normal to the probe axis) is mainly a question of manufacturing tolerances. Isotropy deviations below ± 0.1 dB can be easily achieved. On the other hand, for a rotation of the E-field polarization of a lateral incident plane wave, the probe is no longer symmetric and the influence of the probe material on field components which are parallel or normal to the probe axis is different. Fig.4 shows different field strengths at the sensor location for normal (Fig.4 left) or parallel (Fig.4 right) E-field polarizations. The simulation of probe A in Fig.8 shows the E-field polarization in and around the probe for a 45° polarized incident plane wave in brain tissue. At the sensor location the E-field polarization is rotated by 6° from the axis, resulting in decreased sensitivity for the parallel field components.

Fig.9 shows the measured deviation from isotropy in air and brain tissue simulating liquid of an earlier version of probe A with a geometrically orthogonal sensor arrangement. Since the probe materials have higher permittivities than air but lower permittivities than brain tissue simulating liquid, the effect in air and in simulating liquid is reversed. That the effect is smaller in brain tissue simulating liquid (in Fig.9) is more a coincidence. Other small probes present on the market have shown deviations of up to ± 3.4 dB in solution.

As long as the probe is small compared to the wavelength, the field deflection at the probe boundaries can be regarded as a quasi-static field effect. This means that it depends strongly on the probe materials and design and on the surrounding media, but is largely independent of the frequency or the size of the probe. The effect exists even
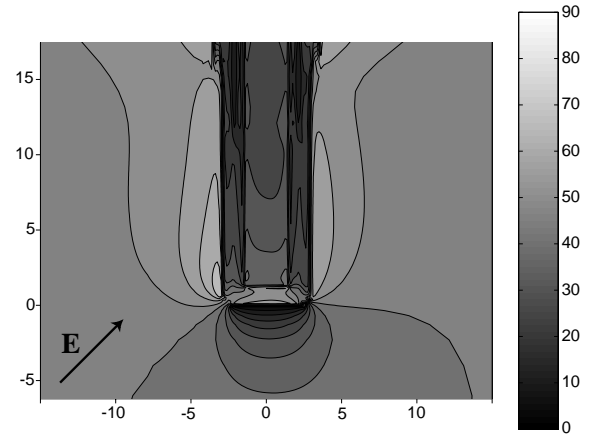

Fig. 8. Angle of the E-field vector on and around the substrate plane for probe A for an incidence with 45° polarized E-field. Dimensions are in mm.
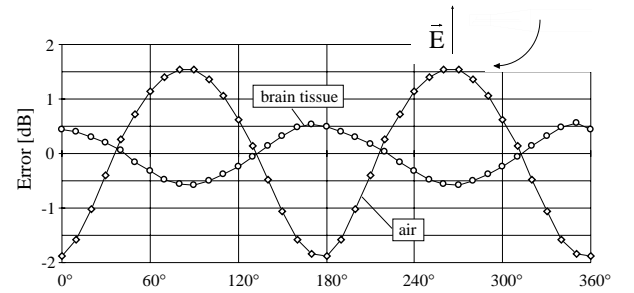

Fig. 9. Deviation from isotropy of an earlier version of probe A in air and in brain tissue simulating liquid at 900 MHz as the E-field was rotated in a plane through the probe axis.

for extremely small probes. Several methods can be used to minimize this effect:

- Using probe materials with parameters similar to those of the surrounding media. The dipoles must be completely suspended in the material.
- Using a spherical probe tip and placing the sensors in the tip center. If the probe body is small compared to the tip, the field deflection is symmetrical for all polarizations.
- Adjusting the angular orientation of the dipole sensors in the probe to compensate for the different sensitivities for normal and axial polarizations. Since this compensation depends on the surrounding media, the probe will be restricted for use in media with similar dielectric parameters.
- Adjusting the sensor sensitivities according to the field orientation towards the probe axis. This is only possible if the E-field component along the probe axis can be separated, i.e., if one of the sensors is aligned to the probe axis.

Since mechanical constraints limit the first two possibilities, the third method was employed in the dosimetric probe designs. Although the angle correction results in a non-orthogonal geometrical arrangement of the sensors, the directivity patterns of the sensors with respect to the external field remain orthogonal. This compensation has been performed for all three probes presented in this paper. In Fig.10 measured deviation from isotropy for probe

A is shown. By rotating the sensor angle 2.7° towards the probe axis (compared to the classical sensor angle - see [1]), the overall isotropy error could be reduced to ±0.25 dB.
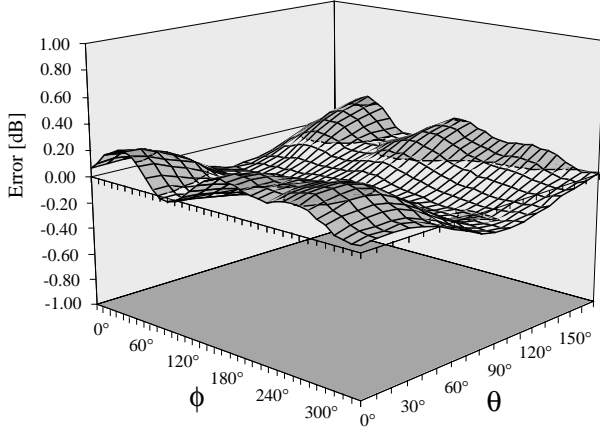

Fig. 10. Overall deviation from isotropy (half sphere) for probe A (optimized sensor angle) measured in brain tissue simulating liquid at 900 MHz (θ is the dipole rotation angle, ϕ is the probe rotation angle). Measurement setup according to Fig.11.

The measurement setup is shown in Fig.11. The probe was positioned at the maximum of the standing wave near the back side of the liquid filled box, where the E-field is partially homogeneous and the H-field is at a minimum. Thus the isotropy error due to the field deflection could be separated from the other isotropy effects described in the following sections.
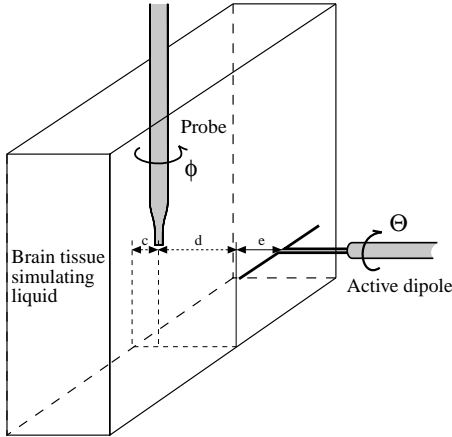

Fig. 11. Setup used to assess the deviation from isotropy in brain tissue simulating liquid (c=2.7 cm, d=7.6 cm and e=3 cm) at 900 MHz.

B. Eddy currents

In the previous section the effect of different permittivities in probe materials and surrounding media is discussed. Totally different problems arise if the probe has a different conductivity than the surrounding media, which is generally the case in dosimetric applications. If a lossless probe is inserted in a lossy media, the probe disrupts the eddy-currents and an electric field builds up at the probe discontinuities. Fig.12 shows a simulation of probe A in brain

tissue between two vertically polarized plane waves moving in opposite directions with opposite polarities. At the probe location the total electric field is canceled and the magnetic field has a maximum. Displayed is the horizontal E-field component as a percentage of the incident E-field for 900 MHz (left) and 1800 MHz (right).
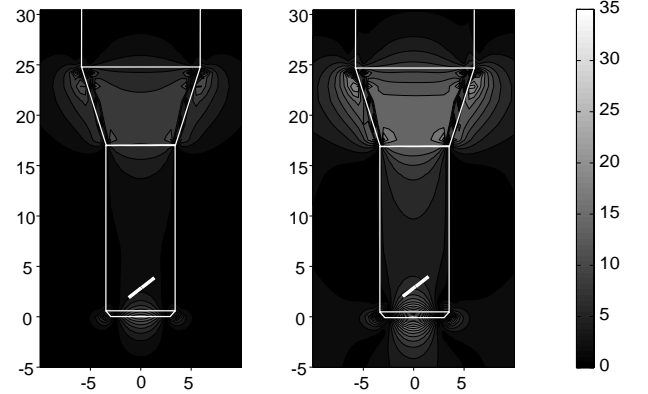

Fig. 12. Horizontal component of the electric field (as a percentage of the incident field) around the simplified probe A inserted between two plane waves moving in opposite directions and with opposite polarities. Dimensions are in mm.

The spurious H-field sensitivity of E-field probe in lossy media can also be seen in the receiving pattern of the probe, when the E-field is kept normal to the probe axis and only the H-field polarization is rotated. The setup in Fig.14 with the dipole normal to the probe axis was used for this measurement. The directivity patterns of probes A and C in brain tissue simulating liquid at 900 MHz are shown in Fig.13. The angle ϕ gives the probe rotation around its axis, ϑ is the probe inclination or the H-field polarization. The variation with ϑ in probe A is due to the eddy-current effect. If the same measurement is done in air, the probe sensitivity is independent of ϑ.
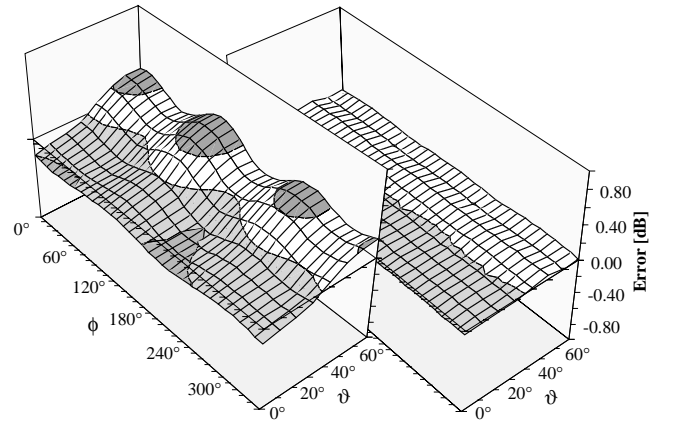

Fig. 13. Directivity patterns of probes A (left) and C (right) in brain tissue simulating liquid at 900 MHz. (The dipole in the setup of Fig.14 was positioned normal to the probe axis.)

The eddy-current effect is not a quasi-static effect and therefore strongly depends on the frequency (see Fig.12) and the probe size. For very small probes the effect disap-
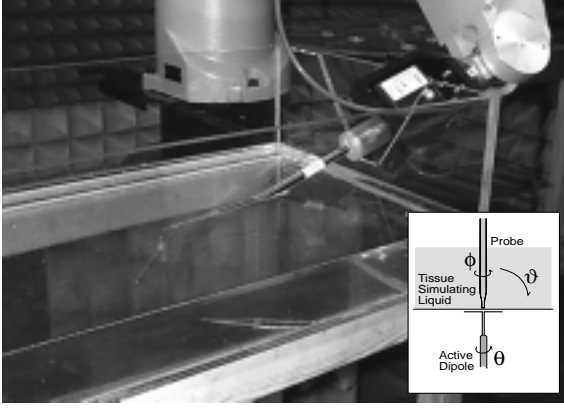
Fig. 14. Test setup used to measure the 3D deviation from isotropy.

pears (see Fig.13 right). Since the effect is frequency and media dependent, a general compensation is not possible. However, if the sensors are located where the H-field induced electric fields in the probe tip are small, the effect can be reduced significantly.

C. Spatial Resolution

The dipole sensors in real probes have finite length and are displaced from the center of the probe. Each sensor measures the field at a different location. This gives an error in the evaluation of the total E-field in inhomogeneous fields with fast changes in magnitude or polarization. Fig.15 shows the setup used to investigate the probe behavior in strong field gradients normal to the probe axis. Two dipoles with opposite polarizations were placed in direct contact with a flat phantom.
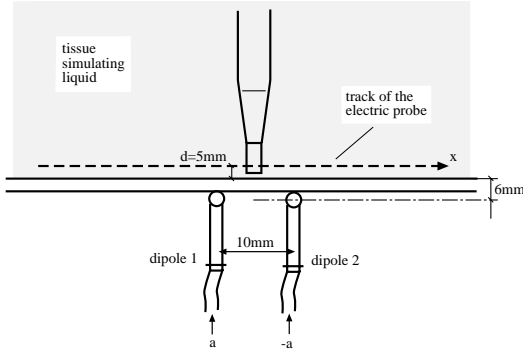

Fig. 15. Sketch of the setup used to investigate the spatial resolution of dosimetric probes.

Fig.16 gives the response along an orthogonal trajectory over the dipole feedpoints for the three probes and their crosssections at the same scale. The different probe readings in the area of the field minimum are due to the sensor displacement and not due to the field integration over the sensors. Each sensor in probe A gives a distinct minimum, but at different probe locations (i.e., one of the sensors always has some signal). In the area of the field maxima the normal field gradients are significantly smaller and all three probes give the same reading.
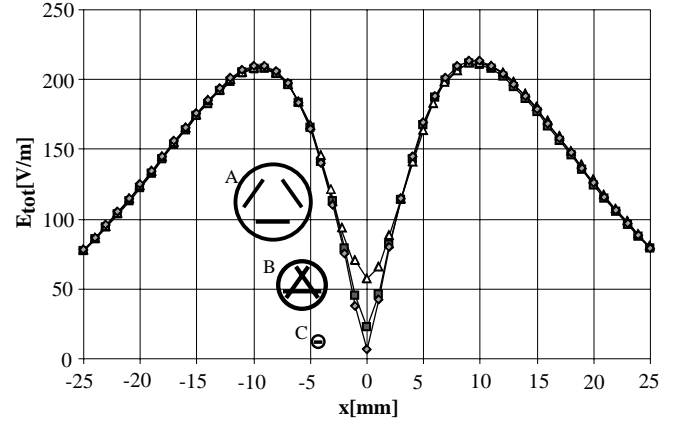

Fig. 16. Total E-field along the x-axis at d=5 mm measured with probe A ($\triangle$), probe B ($\square$) and probe C ($\diamond$). Measurement setup according to Fig.15.

If the probe is rotated around its axis, the sensors move through the field around the probe axis. Fig.17 shows the normalized SAR reading for a probe rotation around the probe axis at x=15 mm in the above setup, where the normal SAR gradient is about 10 % per millimeter. Fig.18 shows the resulting deviation from isotropy. The 120° probe symmetry is clearly visible.
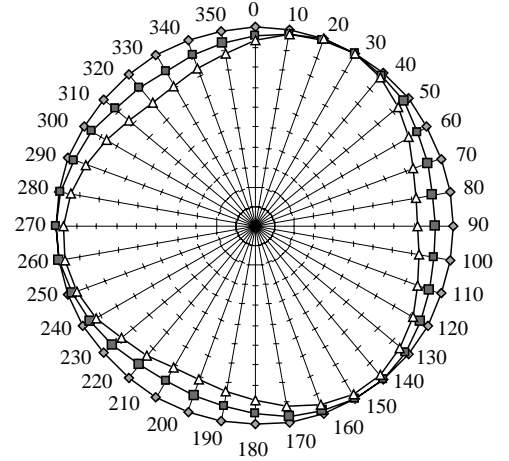

Fig. 17. Rotation at x=15 mm and d=5 mm for probe A ($\triangle$), probe B ($\square$) and probe C ($\diamond$). Measurement setup according to Fig.15.

The deviation from isotropy due to the sensor displacement is proportional to the field gradient normal to the probe axis and is largest for fields polarized in the direction of the sensors. In Fig.10 this isotropy deviation (discernible by the 120° symmetry in the ϕ-direction) is highest for a dipole angle θ between 30° and 40°. The worst case error can be estimated by multiplying the field gradient normal to the probe axis (in % per mm) by the equivalent sensor displacement (in mm). Table II gives the equivalent sensor displacements for the three investigated probes.

Since all sensors have the same offset from the probe tip, the isotropy error disappears if the field gradients are parallel to the probe as shown in Fig.13 for ϑ=0°.
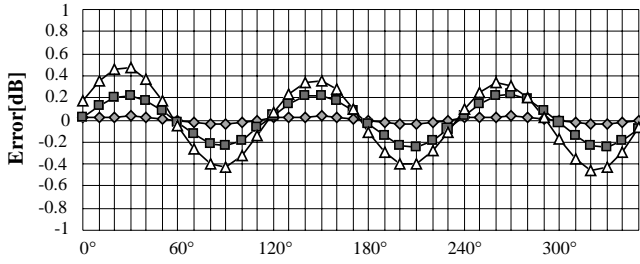
Fields in tissue simulating liquids are generally gradient

Fig. 18. Error of the probe rotation at x=15 mm and d=5 mm for probe A (△), probe B (□) and probe C (◇). Measurement setup according to Fig.15.

TABLE II

EQUIVALENT SENSOR DISPLACEMENT.

| | Sensor displacement | |
Probe	mechanical [mm]	equivalent [mm]
A	1.6	1.1
B	0.56	0.3
C	0±0.1	0.05

fields with a SAR decay between 5 mm and 20 mm in the mobile frequency range. Accurate measurements are only possible if the probe is calibrated at the actual measurement center in the probe, i.e., at the location of the center of the dipole sensor. If a probe with calibration at the mechanical probe tip is used in fields with different gradients, large errors occur because the relations between the field strengths at the tip and at the probe sensors change with the field gradient.

The sensor displacement can produce large measurement uncertainties which are dominant over other uncertainties in well designed probes (see also Table IV). A general compensation for arbitrary fields is not possible, except in making the probe small and placing the sensors close to the center, as in Probe B.

A significant reduction of the measurement uncertainty is possible in certain applications by choosing an appropriate procedure. If a symmetric probe can be used in a way that prevents strong gradients normal to the probe axis, the sensor displacement has little impact on the probe reading. This is the case for measurements in shell phantoms when the probe is oriented mostly normal to the surface. If the main interest is in the field maxima, as for compliance testing, the normal gradients are small. In this application the influence of the sensor displacement even for probe A is negligible compared to other field effects. For general measurements in arbitrary fields, probes B and C clearly show their advantages (see Table IV).

D. Sensor scattering

The metallic sensors in the probe produce a scattered field which will be received by the neighboring sensors. The result is a rotation of the directivity pattern for each sensor similar to the effect of the field deflection. However, the scattering effect is much smaller in magnitude, since

the scattering at the sensors is small compared to the scattering at the material boundaries. This was confirmed for probes A and B. There was no measurable change in the receiving pattern of one sensor after removing the two other sensors. Any remaining effect would be corrected by the compensation method applied for the field deflection in the probe (see above).

IV. FIELD DETECTION

The effects mentioned so far have dealt with the coupling of the RF-field to be measured with the dipole sensors. From there the signals must be transmitted to the data acquisition system through links which are transparent to the measured field. In electrical field probes this is approximated by rectifying the RF-signal with detector diodes at the sensor gap and by using resistive lines to transmit the rectified signal to the preamplifier. Thermal noise and the preamplifier characteristics limit the highest line impedance; thus the actual lines will influence the measured field and the probe characteristics in several ways.

A. Lead pickup

Due to the finite line resistance, the field will induce currents in the line which will flow through the rectifier diode and generate a superimposed sensor output. This spurious reception mode has a high resistive source impedance and affects the probe at lower frequencies where the mainly capacitive dipole sensor and diode have high impedances. It is responsible for the lower frequency limit in the probe but becomes negligible at high frequencies. The distortion due to lead pickup was characterized in detail in [4]. High resistivity and capacity in the line reduce the pickup and the minimum usable frequency of the probe. Thin film technique is mostly used to produce the resistive lines with line widths and separations down to 25 μm. In probes A and B the lines are produced with thick film technique. These structures are much coarser; however the technique allows higher sheet resistances and easy production of different sheet resistances on the same substrate. Both probes use sheet resistances of around 100 kΩ/□ in the sensor vicinity, and 1 kΩ/□ for the remaining line. In probe B the lines are printed one above the other with a printed dielectric layer in between, thus greatly increasing the interlead capacity. In the newer versions of probe A only one line is printed and subsequently separated with a 40 μm longitudinal laser cut. A lumped capacitor additionally short-circuits differential signals picked up by the line. Both probes can be used for frequencies down to 30 MHz.

B. Sensor loading

The wave impedance of the resistive line loads the detector diode. Since the line wave impedance is proportional to $1/\sqrt{f}$ and the diode impedance is proportional to $1/f$, the loading effect results in a non-linear frequency response at lower frequencies.

C. Probe Linearity

Most probes use Schottky detector diodes at the sensor gap for signal detection due to their high sensitivity. At higher frequencies the depletion layer capacitance is dominant in the diode impedance. With the mainly capacitive dipole impedance the frequency response becomes very linear.

On the other hand, detector diodes are highly non-linear over the signal strength. For small signals the detector output voltage is proportional to the square of the RF voltage. At around 100 mV (for low barrier silicon Schottky detector diodes) the output becomes linear to the applied RF voltage. This diode compression can be compensated in the evaluation system if the compression characteristic is known. For modulated RF signals the modulation signal is distorted at the amplifier input due to the low pass characteristics of the resistive lines and the amplifier capacitance with typical cut-off frequencies between 10 Hz and 1 kHz. For a compensation of the diode compression the modulation signal must be reconstructed. This is straight forward if some modulation data is known a priori (e.g., the duty cycle for pulsed signals or the power distribution for CDMA signals).

The variable source impedance of the diode is responsible for the "peak detector" effect in electric field probes. During high signal pulses the diode has a low impedance, thus quickly charging the capacitance of the lines and amplifier inputs. During the following signal break the impedance is high and the discharge is slow. The peak detector effect can be minimized if the timing characteristics of the detected signal is less dependent on the diode impedance. Probes A and B have a line impedance of several MΩ in the first few millimeters after the diode and give an average field reading even for high power pulsed signals.

V. Probe Characterization

For small E-field probes used for free space measurements, the deviation of spherical isotropy is beside sensitivity and linearity the most important characteristic. It can be specified easily, since it is caused mainly by field deflection effects, manufacturing tolerances and line pick-up. These effects do not depend strongly on the (typical) measurement situation, allowing a general estimation of the probe uncertainty.

In lossy media the situation is more complicated. The fields are highly unisotropic with strong gradients and short wavelengths, and the probe responds to more field parameters (H-field, gradient, propagation direction). Many of the described field effects depend on the frequency and the dielectric parameters of the surrounding media. Furthermore, for tissue simulating solutions the dielectrical parameters also change with the frequency. The calibration and isotropy assessment for each frequency must take place in media with equal (or similar) properties as the media it will be used in.

A simplified calibration procedure is presented in [5], where the probe sensitivity is split into the product of the sensitivity in air and the sensitivity enhancement in liquid ('Conversion factor'). The calibration in air characterizes the different sensitivities of each sensor (due to different diode depletion layer capacitances) and the described probe linearity effects, since they do not depend on the surrounding media. The following calibration in liquid (see [3]) determines the conversion factor and the correction parameters for the boundary effect. In symmetric probes, the conversion factor is the same for each sensor. Table III shows the conversion factor in brain simulating liquid for the three probes at 900 and 1800 MHz.

TABLE III
PROBE CONVERSION FACTORS.

Probe	900 MHz	1800 MHz
A	5.9	4.8
B	5.9	5.4
C	13.5	13.1

The table shows for all probes a large enhancement of the sensitivity in tissue simulating liquids. The conversion factors depend more on the construction materials and the probe design than on the probe size. However, if the probe is extremely small, the conversion factor is less frequency dependent and the probe behaves more like a free space probe. The receiving pattern also must be assessed in the corresponding media. Fig.14 shows a setup for assessing the 3D spherical isotropy of the probe in liquids. However, the probe inclination angle is limited to 70°. The field gradient at the probe tip can be adjusted by changing the dipole distance from the phantom and by utilizing the standing waves near the top liquid surface. The setup in Fig.11 can be used to measure the polarization pattern for field propagations normal to the probe. Using synchronized dipoles symmetrically on both sides produces a local homogeneous field in the center of the box.

A complete assessment of the receiving pattern in fields with high gradients will give an estimate of the worst case probe isotropy deviation for any field situation. This general isotropy uncertainty can be relatively large compared to other uncertainties. For example, probe A gives a total spherical isotropy uncertainty of ±0.8 dB at 1800 MHz in brain simulating solutions.

However, the probes are often used in measurement systems or applications, where the field parameters are not arbitrarily distributed. In such situations the probe uncertainty can be assessed by correlating the probe isotropy with the probability distribution of the field parameters. For that purpose the contribution of each individual effect to the total isotropy deviation must be known. These can be assessed by analyzing the receiving patterns from different setups with different field gradients (e.g., Fig.10 and Fig.13 applying different dipole angles and gradients).

VI. Conclusions

For dosimetric probes it is very crucial to have an isotropic response under various field conditions (gradients,

<div align="center">

TABLE IV

PROBE COMPARISON.

</div>

	Probe A	Probe B	Probe C
Frequency range			
- full specifications	300-2000 MHz	200-3000 MHz	300-10000 MHz
- reduced specifications	30-3000 MHz	30-6000 MHz	100-10000 MHz
Boundary effects in shell phantoms			
- error at 1 mm distance	+10 %	+6 %	0 %
- no error (<0.1 dB) at	6 mm	4 mm	1 mm
Isotropy in homogeneous fields			
- optimized sensor angle	38°	43°	40°
- deviation at 900 MHz	±0.25 dB	±0.2 dB	±0.2 dB
- deviation at 1800 MHz	±0.4 dB	±0.3 dB	±0.2 dB
Isotropy in normal gradient fields			
- 900 MHz (15 mm penetration)	±0.5 dB	±0.3 dB	±0.2 dB
- 1800 MHz (8 mm penetration)	±0.8 dB	±0.4 dB	±0.2 dB

polarizations, etc). The standard design using three orthogonally arranged sensors at a more or less arbitrary location in a small probe is not adaptable, unless the probe use is limited to certain field polarizations (e.g., fields normal to the probe). Three other commercially available dosimetric probes (not the ones described in this paper) with orthogonal sensors on a triangular core were measured in brain simulating tissue at 900 MHz. For these probes the deviations of the spherical isotropy in homogeneous fields ranged from ±1.3 dB to ±3.4 dB.

The design of accurate field probes for use in lossy tissue is a challenging task. Various field effects must be considered which depend not only on the probe design but also on the actual measurement situation (frequency, media, etc). A general compensation of these effects for all situations will lead to contradictory design criteria. A probe with extremely low deviation from isotropy must be specially designed for the desired media range (e.g., tissue with high water content) and frequency range (e.g., mobile communication range). The probe construction, the probe materials, the sensor angles and the sensor location in the probe tip must all work together to optimize the performance for the selected application. If the probe is very small, some of the field effects become negligible, thus simplifying the probe design and widening the application range.

The three probes A, B and C were developed for dosimetry in solutions with relative permittivities above 20 and conductivities from 0.5 to 2.5 S/m. This includes solutions simulating tissue with high water content (brain, muscle) and culture-media or saline solutions used in biological experiments. They cannot be used in arbitrary fields in free space, since the spherical isotropy deviations in free space are large (> ± 2 dB). Table IV gives a comparison of some specifications.

Probes A and B are used for design and compliance tests of mobile phones in the DASY3 system [2]. In that application the boundary effect is compensated in the measurement procedure. Since the probe is positioned approximately normal to surface, the main field gradients are par-

allel to the probe and the resulting isotropy deviation is largely reduced. Probe C is mainly used for dosimetry in small animals or cell dishes or as a reference probe in the analysis of other dosimetric probes. Its fragile tip makes it unsuitable for an automated scanning system.

<div align="center">REFERENCES</div>

[1] Howard I. Bassen and Glen S. Smith, "Electric field probes – A review", *IEEE Transactions on Antennas and Propagation*, vol. 31, no. 5, pp. 710–718, Sept. 1983.

[2] Thomas Schmid, Oliver Egger, and Niels Kuster, "Automated E-field scanning system for dosimetric assessments", *IEEE Transactions on Microwave Theory and Techniques*, vol. 44, no. 1, pp. 105–113, Jan. 1996.

[3] Katja Poković, Thomas Schmid, and Niels Kuster, "Robust setup for precise calibration of E-field probes in tissue simulating liquids at mobile communications frequencies", in *ICECOM'97*, Dubrovnik, October 15–17, 1997, pp. 120–124.

[4] Glenn S. Smith, "Analysis of miniature electric field probes with resistive transmission lines", *IEEE MTT*, vol. 29, pp. 1213–1224, 1981.

[5] Klaus Meier, Michael Burkhardt, Thomas Schmid, and Niels Kuster, "Broadband calibration of E-field probes in lossy media", *IEEE Transactions on Microwave Theory and Techniques*, vol. 44, no. 10, pp. 1954–1962, Oct. 1996.